



## RESEARCH LETTER

10.1029/2018GL079423

### Key Points:

- Based on AIRS observations the frequency of extreme (tropopause overshooting) deep convective clouds (DCCs) is expected to increase about 21%/K of warming of the tropical oceans
- The expected increase in the frequency of extreme precipitation in the NCAR CAM5 model is not inconsistent with the increase in frequency of extreme DCCs derived from observations
- Based on the CMIP5 predicted 2.7 K increase in the surface temperature of the tropical oceans, the frequency of extreme DCC could increase by about 60% by the end of this century

### Supporting Information:

- Supporting Information S1
- Figure S1
- Figure S2
- Figure S3

### Correspondence to:

H. H. Aumann,  
hhaumann@jpl.nasa.gov

### Citation:

Aumann, H. H., Behrangi, A., & Wang, Y. (2018). Increased frequency of extreme tropical deep convection: AIRS observations and climate model predictions. *Geophysical Research Letters*, 45, 13,530–13,537. <https://doi.org/10.1029/2018GL079423>

Received 29 JUN 2018

Accepted 28 NOV 2018

Accepted article online 3 DEC 2018

Published online 21 DEC 2018

## Increased Frequency of Extreme Tropical Deep Convection: AIRS Observations and Climate Model Predictions

Hartmut H. Aumann<sup>1</sup> , Ali Behrangi<sup>1,2</sup> , and Yuan Wang<sup>1,3</sup>

<sup>1</sup>Jet Propulsion Laboratory, California Institute of Technology, Pasadena, CA, USA, <sup>2</sup>Department of Hydrology and Atmospheric Sciences, University of Arizona, Tucson, AZ, USA, <sup>3</sup>Division of Geological and Planetary Sciences, California Institute of Technology, Pasadena, CA, USA

**Abstract** Atmospheric Infrared Sounder (AIRS) data from the tropical oceans (30°N to 30°S) are used to derive the probability of the process resulting in deep convective clouds (DCCs) as function of the sea surface temperature (SST). For DCC at or below the tropopause the onset temperature of this process shifts at the same rate as the increase in the mean SST. For tropopause overshooting DCC, which are associated with extreme rain events, the shift of the onset temperature is slower, causing their frequency to increase by about 21%/K of warming of the oceans. This sensitivity is not inconsistent with the sensitivity of the increase of extreme deep convective rain in the National Center for Atmospheric Research Community Atmosphere Model version 5 model for a warmer SST. The mean of the 36 fifth Phase of the Coupled Model Intercomparison Project models predicts a 2.7 K warmer tropical SST by the end of this century, resulting in a 60% increases in the frequency of tropopause overshooting DCC.

**Plain Language Summary** We use 15 years of Atmospheric Infrared Sounder observations of the tropical oceans to derive the probability of the deep convective cloud (DCC) process as a function of the sea surface temperature. Based on this, the frequency of extreme (tropopause overshooting) DCCs will increase about 21% per 1 K of warming of the tropical oceans. Tropopause overshooting DCC are correlated with extreme rain rates. We evaluated the expected increase in the frequency of extreme precipitation in the National Center for Atmospheric Research Community Atmosphere Model version 5 model in a warmer tropical ocean. The increase of extreme rain rates in the model is consistent with the Atmospheric Infrared Sounder-derived increase in frequency of extreme DCC. The mean of the fifth Phase of the Coupled Model Intercomparison Project models predicts a 2.7 K increase in the surface temperature of the tropical oceans by the end of this century. This means that the frequency of extreme DCC in the tropical oceans could increase by about 60%.

### 1. Introduction

The high correlation between extremely cold cloud top brightness temperatures, variously referred to as deep convective clouds (DCCs), detected by infrared sensors from space in the thermal infrared, and extreme rain rates has already been shown (e.g., Arkin & Meisner, 1987; Behrangi et al., 2009; Vicente et al., 1998), especially for the tropical oceans. The rapid increase in the observed frequency of DCC when the sea surface temperature (SST) exceeds 299 K, with a peak near 302 K, followed by a rapid decrease and virtually no DCC at SST warmer than 305 K, has also been studied (e.g., Behrangi et al., 2012; Gadgil et al., 1984; Waliser & Graham, 1993). In a warmer ocean the SST is likely to exceed a threshold temperature at more locations, resulting in an increase in the number of DCC, and hence an increase in extreme rain rates. However, the threshold for the onset of processes related to deep convection may shift with the SST (Sahany et al., 2014; Williams et al., 2009), which may diminish the potential increase. The expected increase in precipitation intensity and frequency of cold clouds has been confirmed using time series analysis of multiple satellite records, but their sensitivities to a change in SST vary from 0 to +45%/K, depending on the definition of extreme rain rate, cold clouds, and the analysis period (Aumann et al., 2008; Johnson & Xie, 2010; Liu & Allan, 2012; Liu et al., 2009; Wentz et al., 2007).

In a time series analysis, the ratio of the anomaly trend in the DCC frequency (change in units of %/year) and the anomaly trend in the mean ocean SST (change in units of K/year) is the sensitivity of the change in the DCC frequency to a change in the SST (in units of %/K). The term “frequency” is defined as the percent of the area of the tropical ocean (latitude 30°S to 30°N) associated with DCC or rain rates. However, the large

interannual variability of the SST complicates the interpretation of the results of a time series analysis. Here we largely bypass the problems of time series analysis by comparing the change in the annual mean frequency of the DCC to the change in the annual mean SST due to interannual variability. This could be done directly, but we opted for a probability density function (PDF) approach. In the PDF approach we derive the probability of the DCC process as function of the SST. This DCC process probability is then applied to the SST distribution function to deduce the sensitivity of the frequency of the DCC frequency to a warmer ocean.

## 2. Data

### 2.1. AIRS

The Atmospheric Infrared Sounder (AIRS, Aumann et al., 2003) was launched in 2002 into a polar orbit on the Earth Observing System (EOS) Aqua spacecraft. AIRS scans cross track from  $-49.5^{\circ}$  to  $+49.5^{\circ}$  in 90 steps every 2.667 s, and 135 scan lines define a 6-min data granule. Each data granule contains  $90 \times 135 = 12,150$  spectra. Each spectrum is associated with a number of supporting data, including latitude, longitude, surface elevation, and the SST. The SST is based on the daily real time global SST product by the National Oceanic and Atmospheric Administration on a  $0.5^{\circ}$  grid (Thiébaux et al., 2003). Of these 12,150 observations two types of spectra were saved for the analysis.

1. Random Nadir Samples (RNSs). From the 12,150 spectra in each granule, we pseudo-randomly selected  $135 \times \cos(\text{latitude})$  observations from within  $3.3^{\circ}$  of nadir. The  $\cos(\text{latitude})$  weight suppresses the spatial overcoverage at high latitudes common to all cross-track scanners. The ratio  $R = 12,150 / (135 \times \cos(\text{latitude}))$  is the sampling thinning factor. The RNS selected by this method each day represent a globally unbiased, area representative sample of the global conditions. Of the global RNS, typically 7,000 RNSs each day are from the tropical oceans. From these data, we created annual data sets of 2.6 million RNS per year, each with the SST, BT1231 and BT1419 for the 15 years from 2003 to 2017 for a PDF analysis. BT1231 is the brightness temperature in the  $1,231 \text{ cm}^{-1}$  atmospheric window channel. BT1419 is the  $1,419\text{-cm}^{-1}$  midtropospheric water vapor sensitive channel. The annual mean SST between 2003 and 2017 ranged from 299.1 to 299.7 K. The warmest 2 years were 2015 and 2016, the coldest 2 years were 2008 and 2011. This is the 99th percentile of the SST for 2016, the warmest of years, was 303.8 K.
2. Extremely cold clouds. If the latitude of the observation is between  $50^{\circ}\text{S}$  and  $50^{\circ}\text{N}$  and BT1231 is less than 225 K (i.e., DCCs), we saved both land and ocean spectra at every scan position. For the analysis we selected the DCC from  $30^{\circ}\text{N}$  to  $30^{\circ}\text{S}$  ocean. Cloud top temperatures close to the climatological tropical tropopause cold point temperature (between 205 and 215 K; cf. Gettelman et al., 2002, Liu et al., 2007) are widely assumed to be indicative of deep convective activity. Cloud tops substantially colder than the climatology cold point are referred to as “overshooting” DCCs. On a yearly average, 11,200 DCCs are saved each day from the tropical oceans. These clouds cover 2% of the tropical oceans; that is, they represent the 98th percentile of cloud top temperatures. The fraction of DCCs associated with the warmest SST dropped from 4.7% to 1.3% to 0.4% for  $\text{SST} > 304, 305, \text{ and } 306$ , respectively. Following Aumann et al. (2011), we used  $DW = \text{BT}1231 - \text{BT}1419$ , the difference between an atmospheric window channels and a water vapor sensitive channel as climatology-independent indicator of the overshoot condition. We divided the observations of DCCs into six groups using a combination of BT1231 and DW as metrics of the strength of the convection. These groups are defined in row#1 of Table 1. For cloud tops colder than 225 K, but warmer than about 208 K, groups#1 and #2 are cold clouds at or below the tropopause. Groups #3 and 4 represent transition groups. Groups #5 and #6 (DCC 5,6) represent the tropopause overshooting DCCs, found in 0.2% of the tropical oceans (99.8th percentile). The extremely cold DCC 5,6 are always surrounded by the warmer DCC 1,2. Table 1, row#2 is the mean DW of the group; row#3 is the frequency of the clouds.

### 2.2. AMSRE

In order to associate rain rates with BT1231 and DW, we used AMSRE data (Advanced Microwave Scanning Radiometer on EOS, Wentz et al., 2014). Since AMSRE is also on the EOS Aqua spacecraft, the data from the daily ascending and descending overpasses match the AIRS data. AMSRE measures the sum of stratiform, convective, and deep convective rain. AMSRE is a conical scanner, while AIRS scans cross track. Consequently, the rain rate reported by AMSRE is measured about 3 to 4 min before AIRS observes the same location. Row#4 in Table 1 is the mean rain rate for each group. It can be seen that the colder the cloud tops,

**Table 1**  
Definition of DCC Groups and Summary of Results

	Group 1: 208 < BT < 225 K and DW >= 0	Group 2: 208 < BT < 225 K and DW < 0	Group 3: 206 < BT < 208 K and DW < 0	Group 4: 203 < BT < 206 K and DW < 0	Group 5: 199 < BT < 203 K and DW < 0	Group 6: BT < 199 K and DW < 0
Mean (DW)	+5.4 K	-0.64 K	-1.15 K	-2.1 K	-3.4 K	-5.7 K
Percent of tropical ocean	1.42%	0.11%	0.092%	0.11%	0.11%	0.11%
AMSRE rain rate (mm/hr)	1.54	2.50	2.57	2.84	3.32	4.50
Percent of total rain	20	2.5	2.1	2.8	3.3	4.5
AIRS DCC false alarm rate	26%	15%	15%	13%	13%	13%
Slope with 0.10 threshold	+0.974 ± 0.275	+0.895 ± 0.374	+0.981 ± 0.152	+0.752 ± 0.119	+0.632 ± 0.121	+0.290 ± 0.085
Slope with 0.15 threshold	+0.979 ± 0.173	+0.919 ± 0.276	+0.803 ± 0.138	+0.711 ± 0.116	+0.541 ± 0.101	+0.278 ± 0.120
Slope with 0.20 threshold	+0.871 ± 0.158	+1.008 ± 0.202	+0.730 ± 0.128	+0.624 ± 0.122	+0.541 ± 0.087	+0.351 ± 0.137
Mean slope (K/K)	+0.90 ± 0.18	+0.94 ± 0.25	+0.80 ± 0.14	+0.68 ± 0.13	+0.52 ± 0.11	+0.27 ± 0.13
Mean onset temperature (K)	299.0	298.8	301.3	301.6	301.8	302.1
Sensitivity without CA	+20%/K	+17%/K	+25%/K	+29%/K	+32%/K	+39%/K
CA corrected sensitivity	+2 ± 4%/K	+2 ± 4%/K	+5 ± 4%/K	+9 ± 4%/K	+15 ± 4%/K	+28 ± 5%/K

Note. BT stands for BT1231. DCC = deep convective cloud; AIRS = Atmospheric Infrared Sounder; AMSRE = Advanced Microwave Scanning Radiometer on the Earth Observing System.

the more negative DW, and the higher the average rain rate. Row#5 is the fraction of the total rain rate in the tropical oceans associated with each group. Cloud tops colder than 225 K account for 35%, the overshooting DCCs account for 7.8% (Table 1, row#5, sum of groups #5 and #6) of the total AMSRE rain rate, respectively.

Row#6 is the false alarm rate. This is the fraction of the DCCs which is associated with a rain rate of less than 0.1 mm/hr, the smallest nonzero AMSRE rain rate. For the tropopause overshooting DCCs we interpret the finite duration of the occurrence of extreme rain rates and a typically 4-min delay between the AMSRE observations and the AIRS measurements as the dominant cause of the 13% false alarm rate. If a rare event, like extreme rain, were to last for 30 min but is observed by AIRS 4 min later than by AMSRE, the probability of AIRS missing the entire event is approximately  $4/30 = 13\%$ .

### 3. AIRS Data Analysis

For the PDF analysis of the data, let  $N_{\text{ocean}}$  be the annual count of the RNS from the tropical oceans. The probability of  $SST = T$  is  $P_{\text{ocean}}(T)$ . By the definition of a histogram, the number of samples at  $SST = T$

$$N_{\text{ocean}}(T) = N_{\text{ocean}} \times P_{\text{ocean}}(T), \quad (1)$$

where  $N_{\text{ocean}}(T)$  is the histogram of the observed  $N_{\text{ocean}}$  evaluated between 285 and 308 K with 0.1 K wide bins.

$N_{\text{DCC}}$  is the count of observations identified as DCC.  $N_{\text{DCC}}(T)$  is the histogram of  $N_{\text{DCC}}$ .  $N_{\text{DCC}}(T)$  depends on the DCC group. The number of DCCs at any SST,  $N_{\text{DCC}}(T)$ , is the product of the number of samples at temperature  $T$  and the conditional probability of a temperature dependent process,  $P_{\text{DCC}}(T)$ , associated with temperature  $T$ .

$$N_{\text{DCC}}(T) = R \times N_{\text{ocean}}(T) \times P_{\text{DCC}}(T) \quad (2)$$

where the factor  $R$  accounts for the fact that the RNS subsampled the tropical oceans. Hence,

$$P_{\text{DCC}}(T) = N_{\text{DCC}}(T) / (R \times N_{\text{ocean}}(T)) \text{ for } N_{\text{ocean}}(T) \gg 0. \quad (3)$$

We refer to  $P_{\text{DCC}}(T)$ , the probability that a DCC is observed at  $SST = T$ , as the DCC process probability.  $P_{\text{DCC}}(T)$  becomes noisy for  $T > 304$  K, since the  $N_{\text{ocean}}(T) \gg 0$  condition of equation (3) is increasingly no longer valid. Figure 1 shows the mean  $P_{\text{DCC}}(T)$  from the 15 years for DCC groups #4, #5, and #6.

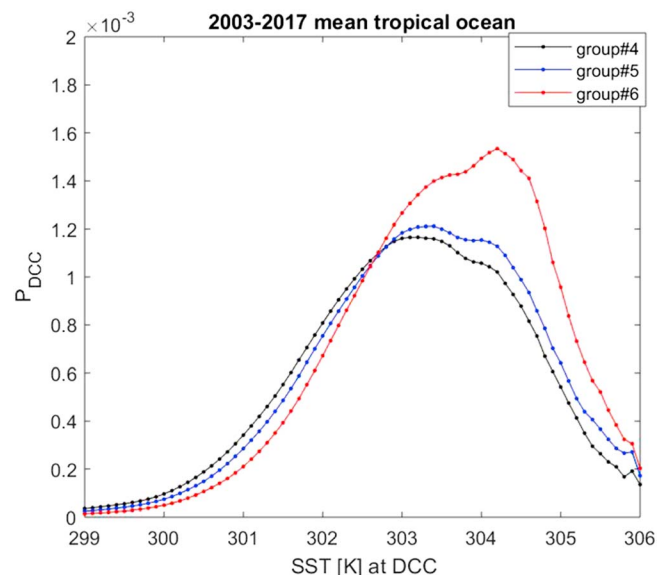


**Figure 1.** The probability that a deep convective cloud (DCC) is observed,  $P_{\text{DCC}}$ , is a function of the sea surface temperature (SST).

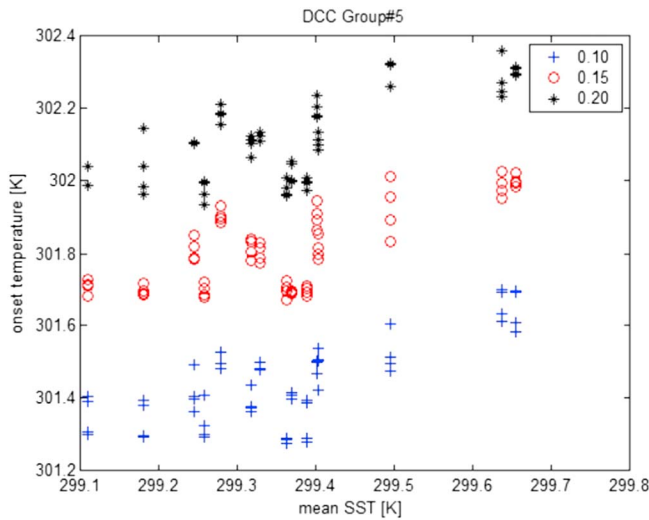


**Figure 2.** The onset of the deep convective cloud (DCC) process for cold clouds in group #5 for 0.1, 0.15, and 0.2 thresholds of the cumulative distribution. SST = sea surface temperature.

the temperature of the onset of the DCC process for three cumulative distribution thresholds, 0.1, 0.15, and 0.2. The scatter in the results from the four independent, but otherwise equivalent groups from each year provides insight into the uncertainties of the numerical procedures.

Figure 2 shows the change of the onset temperature of the DCC process as function of the mean SST for the cold clouds in group #5 for thresholds of the cumulative distribution of 0.10, 0.15, and 0.20. The uncertainty of the onset temperature is given by the scatter in the results for each threshold. It can be seen that the onset temperature of the DCC process occurs at increasingly warmer temperatures as the threshold increases from 0.1 to 0.2. This is expected. More importantly, the slope of the change in the onset temperature with mean SST is consistent for the three thresholds. We refer to the slope of the change (in units of K/K) of the onset of the DCC process with SST as the convective adjustment (CA) of the DCC process.

Table 1, rows 7 through 10, summarizes the CA for the six DCC groups for thresholds of 0.1, 0.15, and 0.20. The intercept between the threshold and CUM (PDF) was calculated using linear interpolation. The number following the “±” is the one sigma confidence CA uncertainty based on the bootstrap method. Row 11 of Table 1 list the mean onset temperatures for each DCC group (average of the three thresholds and the onset temperatures for the 2003 through 2017 data).

Given  $P_{\text{ocean}}(T)$  and  $P_{\text{DCC}}(T)$ , we can use equations (1) and (2) to calculate the frequency of DCC in the current climate and in a warmer climate. For  $N$  observations of the oceans, the number of DCC expected is

$$\sum N_{\text{DCC}}(T) = N \times \sum P_{\text{ocean}}(T) \times P_{\text{DCC}}(T), \text{ summed over all } T. \quad (4)$$

In a  $DT$  K warmer ocean the number of DCCs is given by the

$$\sum N \times P_{\text{ocean}}(T + DT) \times P_{\text{DCC}}(T + CA \times DT). \quad (5)$$

The ratio of these two summations is the fractional change in the DCC frequency between the current and future climate. If  $CA = 1$  the DCC process shifts at the same rate as the SST and there is no change in the number of DCC. If  $CA < 1$  the DCC process shifts warmer at a slower rate than the SST and there will be an increase in the number of DCC. The numerical calculations were done with 0.1 K steps (a shift of one histogram bin) using the 15-year mean  $P_{\text{DCC}}$  and mean  $P_{\text{ocean}}$ . Values for the actual CA were calculated by linear interpolation. For the calculations we averaged the CA calculated for the thresholds of 0.1, 0.15 and 0.2 and used the mean of the slope uncertainties as an estimate of the uncertainty. The results are in row#10 of Table 1.

Rows #12 and #13 of Table 1 summarize the increase in the DCC frequency as the change in the frequency per kelvin increase divided by current mean frequency. The result is a sensitivity in units of %/K for the six DCC

#5, and #6. Groups 5 and 6, referred to as DCC 5,6, are tropopause penetrating DCC.  $P_{\text{DCC}}(T)$  starts to rise steeply at about 300 K. At 303 K the probability is close to 0.0012 (0.12%) for all three groups. For group # 6  $P_{\text{DCC}}(T)$  continues to rise to about 0.0016 (0.16%) near 304.5 K.  $P_{\text{DCC}}(T)$  drops steeply for all three groups to about 30% of the peak value near 305 K, to near zero at 306.5 K.

$P_{\text{DCC}}(T)$  is a function the DCC group. We could define the start of the DCC process as the temperature at which  $P_{\text{DCC}}(T)$  rises above its 1/2 peak value. This definition is intuitively reasonable, but, as seen from Figure 1, the temperature of the peak of  $P_{\text{DCC}}(T)$  is not well defined. We opted to define the onset temperature using the cumulative distribution of  $P_{\text{DCC}}(T)$ , CUM ( $P_{\text{DCC}}(T)$ ). The 1/2 peak threshold for  $P_{\text{DCC}}(T)$  corresponds to a threshold of about 0.15 for CUM ( $P_{\text{DCC}}(T)$ ). For the calculation of the cumulative distribution we set  $P_{\text{DCC}}(T > 305 \text{ K}) = 0$ . This assumption is not critical.  $P_{\text{DCC}}(T > 306 \text{ K}) = 0$  produces almost indistinguishable results.

For each of the 15 years we calculated the mean annual SST values. We then randomly divided the SST at the DCC locations in each of the 15 years into four sets. This gives us  $15 \times 4 = 60$  independent data sets for the calculation of the DCC process probability (equation (3)). We also evaluated

groups. Row#12 gives the sensitivity assuming  $CA = 0$ ; Row#13 gives the CA-corrected sensitivity with the uncertainty based on the uncertainty of CA. For overshooting DCC (mean of groups #5 and #6, representing the extreme 99.8th percentile), corrected for the mean CA of  $0.4 \pm 0.1$  K/K, the mean sensitivity is  $+21 \pm 7\%/K$ .

#### 4. Climate Models

The average of 36 fifth Phase of the Coupled Model Intercomparison Project (CMIP5) state-of-the-art climate model simulations from the CMIP5 (Taylor et al., 2012) under the RCP 8.5 scenario predicts a 2.7 K warming of the tropical oceans between the current climate (1976–2005) and the climate at the end of this century (2070–2100; supporting information section S3). In order to evaluate if the increase in extreme deep convection with warming SST deduced from the AIRS observations is seen in climate models, we made use of the correlation between extremely cold cloud tops and extreme rain rates. For this we examined the extreme precipitation response to the warming SST in the National Center for Atmospheric Research (NCAR) Community Atmosphere Model version 5 (CAM5, Hurrell et al., 2013). As a participating model in CMIP5, the CAM5 has been extensively evaluated (e.g., Gustafson et al., 2014) and is widely used to examine the precipitation variations in response to different radiative forcing (Sahany et al., 2014; Wang et al., 2015). This model also allows a distinction between stratiform, shallow convective, and deep convective precipitation, although deep convection is primarily parameterized as a function of the Convective Available Potential Energy.

In the discussion of the false alarm rate (Table 1, row#6) we noted that DCC are correlated with extreme precipitation, but the duration of extreme rain events appears to be less than 1 hr. The conventional 24-hr-averaged sampling of model outputs may thus result in deficiencies in predicting precipitation extremes (Stephens et al., 2010). More recently, Wang et al. (2016) developed an in situ diagnostic method to generate precipitation PDFs based on precipitation rates at each model time step (the hourly time scale), which significantly facilitates the comparison between Global Circulation Models and satellite observations of transient precipitation rates. The NCAR/DOE Community Earth System Model version 1.2.1 (CESM1) CAM5 was run in the in situ diagnostic mode with one degree horizontal bins for the present-day ocean and for a 2 K warmer ocean, both with a 1-year spin-up and a 6-year integration. The total rain rate in the tropical oceans increased 3.6%/K and total water vapor increased 8.7%/K. A deep convective rain rate in excess of 2 mm/day represents the 69.2th percentile of the tropical ocean bins, which changed to the 67.8th percentile in a 2 K warmer ocean. This corresponds to a sensitivity of  $((100 - 67.8)/(100 - 69.2) - 1)/2 = +2.3\%/K$ . Deep convective rain in excess of 20 and 31 mm/day represents the 98th and 99.8th percentiles. The frequency of these cases increased with a sensitivity of +4%/K and +20%/K, respectively.

#### 5. Discussion

Characterizing the DCC process for six DCC groups based on surface temperature, onset temperature, and CA alone, all derived from 30°N to 30°S data, is clearly an oversimplification. For a first-order test of the ocean area sensitivity we derived CA using 15°N to 15°S data, that is, the deep tropical oceans. Details for DCC group#5 are in supporting information section S2. The mean SST of this zone is 1.3 K warmer than that of the 30°N to 30°S zone. The number of cases in all six DCC groups between 15°N and 15°S is about 30% less than in the 30°N to 30°S region, while the area decreases by about 50%. The mean onset temperatures of DCC groups 1, 2, and 3 changed to the mean SST, while the onset for DCC groups 4, 5, and 6 agreed within 0.1 K with those derived from the 30°N to 30°S zone. The CA from the 15°N to 15°S region agreed within the error bars with the 30°N to 30°S results. Supporting information section S2 includes an additional verification of the stability of the CA result based on a Monte Carlo type test.

Previous studies (e.g., Williams et al., 2009; Sahany et al., 2014) have argued that the threshold for the onset of processes related to convection will shift with the temperature and the vertical profiles controlling convective stability. The magnitude of this shift depends on the process. Johnson and Xie (2010) used a time series analysis to show that between 1980 and 2009 the SST threshold for rain rates larger than 2 mm/day increased at the same rate in kelvin per decade as the tropical mean SST; that is, the CA is near perfect,  $CA = 1$  K/K. They also claimed that the theoretically predicted shift of the moist adiabatic lapse rate (MALR) at 300 hPa of 0.43 K/K is consistent the MALR for the mean of 10 CMIP3 models. It is interesting to note that  $CA = 1$  K/K for the 2 mm/day rain rate threshold is consistent with the CA deduced from our observations of DCC at or below the tropopause (dominated by group#1, Table 1), while  $CA = 0.5$  K/K for the MALR is consistent with our observations of extreme DCC well above the tropopause.

As illustrated with Figure 1,  $P_{DCC}(T)$  for extreme DCCs drops to 30% of its peak value near 305 K, to effectively 0 at 306.5 K. This pattern may be related to convective stability. Extreme DCCs with  $CA < 1$  are always surrounded by less extreme DCCs with  $CA = 1$ . At some future warmer SST the onset of extreme DCCs could equal the onset of the surrounding DCCs at or below the tropopause. The SST where this starts to occur can be estimated from our data. Table 1, row #11, lists the mean onset temperature of the DCC process as function of the DCC group. Assume  $CA = 1$  for moderate DCC and  $CA = 0.5$  for extreme DCC. When the SST warms by 6 K, the onset of the moderate DCC will shift from the present 299 to 305 K, while the onset of the extreme DCC will shift from 302 K to 305 K. At an SST warmer than 305 K the presence of extreme DCCs becomes inconsistent with convective stability; that is, extreme DCCs will no longer form. It is interesting to note that at an SST of about 303 K the heat loss due to evaporation from the cloud-free ocean exceeds the solar input (Hartmann & Michelsen, 1993).

The comparison of the DCCs and the NCAR deep convective rain results is complicated by the uncertainty of the equivalence of the 98th and 99.8th percentiles for the DCCs and the NCAR model rain. With the assumption that the 98th and 99.8th percentiles of the DCCs could be equivalent to ranges from 97 to 99 and 99.5 to 99.9, respectively, in the NCAR model, the NCAR model sensitivities, stated earlier as +4%/K and +20%/K, range from +3%/K to +8%/K and +13%/K to +26%/K, respectively. The ranges resulting from the assumed uncertainties of the percentile equivalents are not 1 sigma confidence limits. We conclude that the sensitivity in the extreme precipitation frequency in the NCAR CAM5 model is not inconsistent with the SST sensitivity deduced for the 98th and 99.8th percentile of the moderate and extreme DCCs.

The sensitivity for overshooting DCCs is more than 2 times larger than the Clausius Clapeyron sensitivity. Allan and Soden (2008) came to a similar conclusion based on the analysis of extreme rain rates in the 1987–2004 Special Sensor Microwave Imager data. The overshooting DCCs account for 7.8% of the total rain rate (Table 1, row#5, sum of groups #5 and #6). Other factors being equal, a 21%/K increase in the frequency of overshooting DCCs may increase their contribution to the total rain rate by 1.6%/K ( $7.8 \times 0.21$ ).

In the introduction we mentioned that the sensitivity of the DCC frequency to a warmer ocean can be calculated directly. In supporting information section S1 we show that this results in sensitivities of  $+2 \pm 6\%/K$ ,  $-12 \pm 15\%/K$ ,  $+1 \pm 8\%/K$ ,  $+15 \pm 9\%/K$ ,  $21 \pm 10\%/K$ , and  $+34 \pm 15\%/K$  for DCC groups #1 through #6 respectively, consistent within the error bars with the PDF results shown in Table 1. The DCC 5,6 directly derived sensitivity is  $+27 \pm 9\%/K$ .

For the calculation of what happens to the frequency of tropopause penetrating DCC (DCC 5,6) in the 2.7 K warmer oceans predicted by CMIP5, we need to consider the evolving shape of the PDF of the SST of the tropical oceans, the PDFs of the DCC processes, and convective stability. The PDF of the tropical SST of the CMIP5 models (supporting information section S3) in a 2.7 K warmer ocean is nearly identical to the PDF of the current climate but shifted 2.7 K warmer: The mean SST will shift from 299.4 K (2003–2017 mean) to 302.1 K. The onset of the DCC 1,2 will shift from present 299 K to  $299 + 2.7 = 301.7$  K, while the onset of the DCC 5,6 process will shift to  $302 + 2.7 \times 0.5 = 303.3$  K. The onset of DCC 5,6 at a warmer temperature than DCC 1,2 is consistent with tropical convective stability.

There are several methods for calculating the likely increase in the frequency of DCC 5,6 and associated uncertainty due to the CMIP5 predicted 2.7 K increase in the SST. The linear extrapolation of the frequency sensitivities derived from the PDF and direct methods for a 2.7 K warming results in a frequency increase between  $+57 \pm 11\%$  and  $+73 \pm 24\%$ , respectively. Use of equations (4) and (5) avoids potential issues of extrapolating sensitivities but assumes that in a 2.7 K warmer ocean the mean  $P_{DCC}$  is shifted  $2.7 \times CA$  K warmer, with  $CA = 0.4 \pm 0.1$ . If we shift  $P_{DCC}$  from  $2.7 \times (0.4 - 0.1)$  to  $2.7 \times (0.4 + 0.1)$ , the DCC frequency increases from 52% to 81%. If we assume that the  $\pm 0.1$  uncertainty in the CA is Gaussian distributed, we find a DCC frequency increase of  $+70 \pm 11\%$ . We conclude that the frequency of tropopause overshooting DCCs may increase by about 60% by the end of this century.

## 6. Summary

We used 15 years of AIRS data from the tropical oceans (30°S to 30°N) to identify cloud tops colder than 225 K. Of particular interest are the DCCs which overshoot the climatological tropopause. They represent the extreme 99.8th percentile of cloud top temperatures and they are associated with extreme rain events.

The probability of the DCC process is a function of the SST and differs for cloud tops below and above the tropopause. The temperature of the onset of the DCC process shifts with the mean SST, referred to as CA. For DCCs at or below the tropopause, the onset temperature shifts at close to the same rate as the increase in the mean SST. For tropopause overshooting DCCs, the onset temperature shifts warmer at a slower rate than the warming of the ocean. As a result the frequency of tropopause overshooting DCCs will increase by about 21%/K of mean warming of the SST. This sensitivity to a change in the SST is not inconsistent with the increase in the 99.8th percentile of deep convective rain predicted by the NCAR CAM5 model equipped with in situ rain rate PDF diagnostics. The mean of the 36 CMIP5 models predicts a warming of the tropical ocean SST by the end of this century to about 303 K. Based on the AIRS data analysis and the CMIP5 prediction, the frequency of tropopause overshooting DCCs may increase by about 60% by that time.

### Acknowledgments

The research described in this paper was carried out at the Jet Propulsion Laboratory, California Institute of Technology, under a contract with the National Aeronautics and Space Administration. We are grateful for the unwavering support of Ramesh Kakar of NASA Headquarters. We acknowledge the helpful comments of an anonymous reviewer on the subject of convective stability. The daily collection of AIRS DCC, merged with the NOAA SST, is found in the AIRS Calibration Data Subset (ACDS), available freely from the Goddard Earth Sciences Data and Information Services Center at <https://disc.gsfc.nasa.gov/AIRS>. The NCAR CAM5 simulations were conducted on the NASA Pleiades supercomputer. The CESM source code can be downloaded from <http://www.cesm.ucar.edu/>. The AMSRE data are freely available from [ftp://ftp.remss.com/amsre/bmaps\\_v07/](ftp://ftp.remss.com/amsre/bmaps_v07/). The CMIP5 RCP 8.5 data can be downloaded from [cmip-pcmdi.llnl.gov/cmip5/data\\_portal.html](http://cmip-pcmdi.llnl.gov/cmip5/data_portal.html). They are served free of charge by the Earth System Grid Federation (ESGF). The RTGSST is freely available from [ftp://polar.ncep.noaa.gov/pub/history/sst/rtg\\_low\\_res](ftp://polar.ncep.noaa.gov/pub/history/sst/rtg_low_res).

### References

- Allan, R. P., & Soden, B. J. (2008). Atmospheric warming and the amplification of precipitation extremes. *Science*, 321(5895), 1481–1484.
- Arkin, P. A., & Meisner, B. N. (1987). The relationship between large-scale convective rainfall and cold cloud over the Western-Hemisphere during 1982–84. *Monthly Weather Review*, 115(1), 51–74. [https://doi.org/10.1175/1520-0493\(1987\)115<0051:TRBLSC>2.0.CO;2](https://doi.org/10.1175/1520-0493(1987)115<0051:TRBLSC>2.0.CO;2)
- Aumann, H. H., Chahine, M. T., Gautier, C., Goldberg, M., Kalnay, E., McMillin, L., et al. (2003). AIRS/AMSU/HSB on the Aqua mission: Design, science objectives, data products and processing systems. *IEEE Transactions on Geoscience and Remote Sensing*, 41(2), 253–264. The AIRS Calibration Data Subset (ACDS) is a daily product freely available from the GSFC DIS. It includes the spectra of all clouds colder than 225K and their associated SST and a random sampled SST. <https://doi.org/10.1109/TGRS.2002.808356>
- Aumann, H. H., DeSouza-Machado, S.G., & Behrangi, A. (2011). Deep convective clouds at the tropopause, ACP.1.1–10. <https://doi.org/10.5194/acp-11-1-2011>
- Aumann, H. H., Ruzmaikin, A., & Teixeira, J. (2008). Frequency of severe storms and global warming. *Geophysical Research Letters*, 35, L19804. <https://doi.org/10.1029/2008GL034562>
- Behrangi, A., Hsu, K.-I., Imam, B., Sorooshian, S., Huffman, G. J., & Kuligowski, R. J. (2009). PERSIANN-MSA: A precipitation estimation method from satellite-based multispectral analysis. *Journal of Hydrometeorology*, 10(6), 1414–1429. <https://doi.org/10.1175/2009JHM1139.1>
- Behrangi, A., Kubar, T., & Lambrigtsen, B. (2012). Phenomenological description of tropical clouds using CloudSat cloud classification. *Monthly Weather Review*, 140(10), 3235–3249. <https://doi.org/10.1175/MWR-D-11-00247.1>
- Gadgil, S., Joseph, P. V., & Joshi, N. V. (1984). Ocean-atmosphere coupling over monsoon regions. *Nature*, 312(5990), 141–143. <https://doi.org/10.1038/312141a0>
- Gettelman, A., Salby, M. L., & Sassi, F. (2002). Distribution and influence of convection in the tropical tropopause region. *Journal of Geophysical Research*, 107(D10), 4080. <https://doi.org/10.1029/2001JD001048>
- Gustafson, W. I. Jr., Ma, P.-L., & Singh, B. (2014). Precipitation characteristics of CAM5 physics at mesoscale resolution during MC3E and the impact of convective timescale choice. *Journal of Advances in Modeling Earth Systems*, 6, 1271–1287. <https://doi.org/10.1002/2014MS000334>
- Hartmann, D. L., & Michelsen, M. L. (1993). Large-scale effects on the regulation of the tropical sea surface temperature. *Journal of Climate*, 6(11), 2049–2062. [https://doi.org/10.1175/1520-0442\(1993\)006<2049:LSEOTR>2.0.CO;2](https://doi.org/10.1175/1520-0442(1993)006<2049:LSEOTR>2.0.CO;2)
- Hurrell, J. W., Holland, M. M., Gent, P. R., Ghan, S., Kay, J. E., Kushner, P. J., et al. (2013). The community earth system model: A framework for collaborative research. *Bulletin of the American Meteorological Society*, 94(9), 1339–1360. <https://doi.org/10.1175/BAMS-D-12-00121.1>
- Johnson, C. N., & Xie, S.-P. (2010). Changes in the sea surface temperature threshold for tropical convection. *Nature Geoscience*, 7. <https://doi.org/10.1038/NGEO1008>
- Liu, C., & Allan, R. P. (2012). Multisatellite observed responses of precipitation and its extremes to interannual climate variability. *Journal of Geophysical Research*, 117, D03101. <https://doi.org/10.1029/2011JD016568>
- Liu, C., Zipser, E. J., & Nesbitt, S. W. (2007). Global distribution of tropical deep convection: Different perspectives from TRMM infrared and radar data. *Journal of Climate*, 20(3), 489–503. <https://doi.org/10.1175/JCLI4023.1>
- Liu, S. C., Fu, C., Shiu, C.-J., Chen, J.-P., & Wu, F. (2009). Temperature dependence of global precipitation extremes. *Geophysical Research Letters*, 36, L17702. <https://doi.org/10.1029/2009GL040218>
- Sahany, S., Neelin, J. D., Hales, K., & Neale, R. B. (2014). Deep convective transition characteristics in the NCAR CCSM and changes under global warming. *Journal of Climate*, 27(24), 9214–9232. <https://doi.org/10.1175/JCLI-D-13-00747.1>. AMS Journal Link.
- Stephens, G. L., L'Ecuyer, T., Forbes, R., Gettelman, A., Golaz, J.-C., Bodas-Salcedo, A., et al. (2010). Dreary state of precipitation in global models. *Journal of Geophysical Research*, 115, D24211. <https://doi.org/10.1029/2010JD014532>
- Taylor, K. E., Stouffer, R. J., & Meehl, G. A. (2012). An overview of CMIP5 and the experiment design. *Bulletin of the American Meteorological Society*, 93(4), 485–498. <https://doi.org/10.1175/BAMS-D-11-00094.1> Model outputs were collected from the Earth System Grid Federation (ESGF) Peer-to-Peer (P2P) enterprise system, Representative Concentration Pathways (RCP) of 8.5. Retrieved from <https://pcmdi.llnl.gov/projects/esgf-llnl/>
- Thiébaux, J., Rogers, E., Wang, W., & Katz, B. (2003). A new high-resolution blended real-time global sea surface temperature analysis. *Bulletin of the American Meteorological Society*, 84(5), 645–656. <https://doi.org/10.1175/BAMS-84-5-645>
- Vicente, G. A., Scofield, R. A., & Menzel, W. P. (1998). The operational GOES infrared rainfall estimation technique. *Bulletin of the American Meteorological Society*, 79(9), 1883–1898. [https://doi.org/10.1175/1520-0477\(1998\)079<1883:TOGIRE>2.0.CO;2](https://doi.org/10.1175/1520-0477(1998)079<1883:TOGIRE>2.0.CO;2)
- Waliser, D. E., & Graham, N. E. (1993). Convective cloud systems and warm-pool sea surface temperatures: Coupled interactions and self-regulation. *Journal of Geophysical Research*, 98, 12,881–12,893. <https://doi.org/10.1029/93JD00872>
- Wang, Y., Jiang, J. H., & Su, H. (2015). Atmospheric responses to the redistribution of anthropogenic aerosols. *Journal of Geophysical Research: Atmospheres*, 120, 9625–9641. <https://doi.org/10.1002/2015JD023665>
- Wang, Y., Ma, P.-L., Jiang, J. H., Su, H., & Rasch, P. J. (2016). Towards reconciling the influence of atmospheric aerosols and greenhouse gases on light precipitation changes in eastern China. *Journal of Geophysical Research: Atmospheres*, 121, 5878–5887. <https://doi.org/10.1002/2016JD024845>

- Wentz, F.J., Meissner, T., Gentemann, C., & Brewer, M. (2014). Aqua AMSR-E. Remote sensing systems, Santa Rosa, CA. Retrieved from [www.remss.com/missions/amr](http://www.remss.com/missions/amr)
- Wentz, F. J., Ricciardulli, L., Hilburn, K., & Mears, C. (2007). How much more rain will global warming bring? *Science*, *317*(5835), 233–235. <https://doi.org/10.1126/science.1140746>
- Williams, I. N., Pierrehumbert, R. T., & Huber, M. (2009). Global warming, convective threshold and false thermostats. *Geophysical Research Letters*, *36*, L21805. <https://doi.org/10.1029/2009GRL039849>